Improved switching performance of a Molybdenum Oxide-based bi-layer resistive memory

Tongjun Zhang[a*], Kai Sun[b], Ioannis Zeimpekis[c] and Ruomeng Huang[a]

Email:tz1n18@soton.ac.uk

***Abstract*— In this paper, an atomic layer deposited memristor based on Al_2O_3/MoO_3 bi-layer structure is reported. Compared with the single layer MoO_3 based device, the bi-layer memristor demonstrates the improved bipolar switching behaviors including better endurance, higher ON/OFF ratio, and higher uniformity of the programming voltages. Space-charge-limited current (SCLC) model is used to explain the current conduction in our memristor. The formation and rupture of conductive oxygen vacancy-based filaments are illustrated as the proposed mechanism for the observed resistive switching behavior.**

Keywords— Resistive memory, MoO_3, atomic layer deposition, bipolar switching

I. Introduction

Breaking the physical and technological limitations of conventional flash-based memory, the novel resistive random-access memory (ReRAM) is triggering researchers' investigation because of its faster operation speed, higher packaging density and lower energy consumption [1]. A typical ReRAM structure consists of two conductive electrodes and a layer of insulator sandwiched between these two electrodes [2, 3]. Generally, the resistive memory device exhibits the ability that can be switched between low resistance states (LRS) and high resistance state (HRS) under different external voltage signals. The properties of the insulating layer play an important role in the resistive switching behaviors of ReRAM. One of the representative material groups that has been widely used in ReRAM development is transition metal oxide dielectric material, such as TaO_2 [4], TiO_2 [5], ZrO_2 [6] and Al_2O_3 [7]. Molybdenum trioxide, MoO_3, is a novel transition metal oxide that has recently attracted significant attention as a resistive switching material. Compared with other transition metal oxide, MoO_3 has relatively wide work function and high dielectric constant. Such material properties could contribute in achieving higher ON/OFF ratio and avoiding extra power consumption [1, 2]. Several MoO_3 based resistive memory have been demonstrated[8, 9]. However, the high programming voltage (above ±2.5 V) and reproducibility of resistive switching in nanoscale devices are main issues researchers facing [10]. Although some groups tried to deposit the MoO_3 layer directly on the bottom electrode directly by using atomic layer deposition (ALD) , the electrical properties are not admirable enough for the application [11]. Therefore, there is currently intense research on nanoscale MoO_3 resistive memory devices with the aim to achieve high switching quality.

This work presents, for the first time, the resistive switching behaviors of transfer-free atomic layer deposited Al_2O_3/MoO_3 bilayer devices. Sandwiched between two TiN electrodes, the memory cells exhibit enhanced bipolar resistive switching behaviors with low programming voltages, narrow switching voltage distribution and good endurance. The possible conduction mechanism and conduction model are also discussed in the results section.

II. Experimental Section

The schematic of the single layer $TiN/MoO_3/TiN$ and the bilayer $TiN/Al_2O_3/MoO_3/TiN$ device are shown in Fig. 1. A 200 nm thick TiN film was reactively sputtered onto the SiO_2/Si substrate to form the bottom electrode in a nitrogen/Argon gas atmosphere. This step was followed by the growth of 30 nm thick MoO_3 layer using thermal atomic layer deposition (ALD) process. The precursors used in this step are bis(tert-butylimido)bis(dimethylamido)molybdenum and ozone [12]. For the bi-layer device, a 20 nm thick Al_2O_3 layer was deposited on the MoO_3 layer by ALD. Then the TiN top electrode was deposited by sputtering and patterned by a shadow mask.

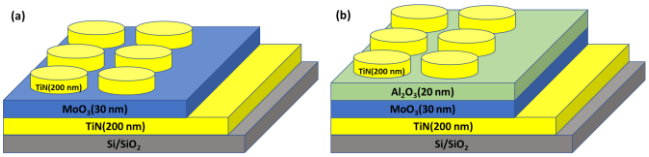

Figure 1. Schematic illustrations of the $TiN/MoO_3/TiN$ single layer device (a) and $TiN/Al_2O_3/MoO_3/TiN$ bilayer device (b).

III. Results and Discussion

Fig. 2a shows the atomic force microscopy surface morphology of the bare MoO_3 film on the TiN electrode with 500 nm × 500 nm scanning window. As can be found in the AFM image, the MoO_3 film consists of small grains with sizes of around 10-20 nm that are uniformly distributed over the surface the MoO_3 layer. The average roughness of the surface is measured to be 1.78 nm. Fig. 2b presents the optical characteristics of deposited MoO_3 thin film on TiN. The refractive index (n) and extinction coefficient (k) are modelled from the ellipsometry data (not shown). The measured optical properties agree with measurement results from MoO_3 samples on silicon substrates [13]. The composition of the MoO_3 thin film was investigated using X-Ray Photoelectron Spectroscopy

[a]Tongjun Zhang and Ruomeng Huang are with the School of Electronics and Computer Science, University of Southampton, Southampton, United Kingdom.

[b]Kai Sun is with the School of Physics, University of Southampton, Southampton, United Kingdom

[c]Ioannis Zeimpekis is with the Optoelectronics Research Centre, University of Southampton, Southampton, United Kingdom

(XPS). The film composition was found to be $MoO_{2.7}$, indicating a deficiency in oxygen. Fig. 2c depicts the of XPS spectrum of the as-deposited MoO_3 film. The peaks at 233 eV and 236.4 eV represent the doublets for the Mo^{6+} oxidation state. In addition, as observed from the characteristic curves of Mo $3d_{5/2}$ level and Mo $3d_{3/2}$ level, the significant peaks can be exported at 232.5 eV and 235.7 eV, respectively. The measured and fitted peaks are corresponded to the Mo^{5+} ions based on the comparison with the standard values. This indicates the potential existence of MoO_2 in the film [14]. The ratio of the peaks implies a MoO_3/MoO_2 ratio of 2.1. The O 1s spectrum is shown in Fig. 2d showing two main component signals (labelled as A and B). The peak A illustrates the lattice oxygen at 531.1 eV and the peak B depicts the interstitial oxygen in MoO_3 at 532.0 eV, respectively [15].

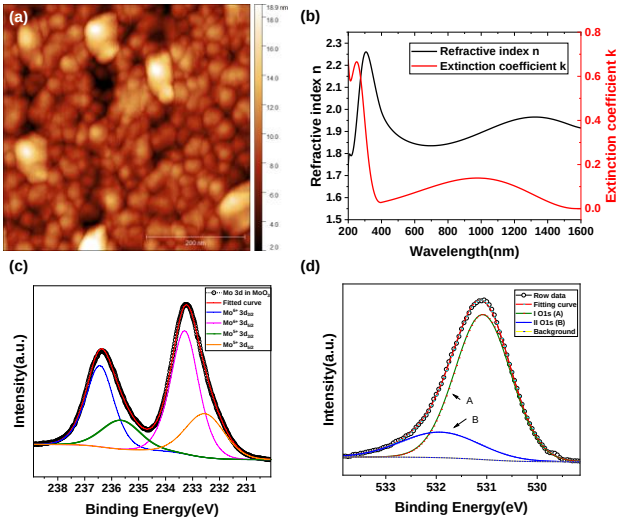

Figure 2. (a) 2D topological measurement results of the MoO_3 layer obtained from AFM tapping mode; (b) Optical constants fitted from the Ellipsometry date for the MoO_3 layer; (c) XPS spectrum and fitting curve of Mo 3d core level region and (d) XPS spectrum and fitting curve of the O 1s core level region.

The electrical characteristics of the single MoO_3 layer-based memristor was first explored by applying DC sweeps over the TiN electrodes. The device is characterised by a forming-free property. This is likely due to the high level of oxygen vacancy in the as-deposited film. A DC sweep with the bias of +2 V and -2 V was applied to the cell and the compliance current (CC) was set as 500 µA in both SET process and RESET process to avoid device breakdown.

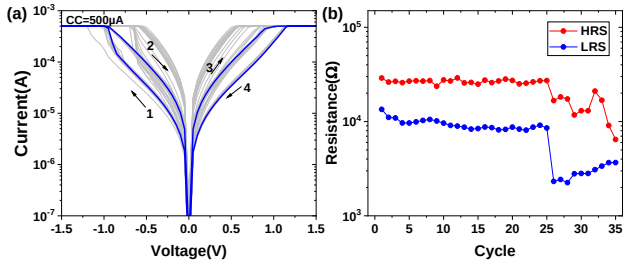

Figure 3. Resistive switching behaviors of the TiN/MoO_3/TiN single layer memory cell. (a) I–V characteristics of the device; (b) The endurance of the device with 35 cycles.

The memristor demonstrates a negative SET behavior as the current increases gradually with the increasing negative potential as shown in Fig. 3a. Then the device was switched off by applying a positive voltage sweep. Thus, these I−V curves demonstrate a typical bipolar switching behaviors where the switching between HRS and LRS can be obtained by applying DC sweeps with different polarities. The DC endurance of the single layer device is presented in Fig. 3b. The device is characterised by a small ON/OFF ratio (*ca.* 3) and a clear drift of both HRS and LRS can be observed after the 26^{th} cycle.

In order to improve the electrical properties of the single MoO_3 layer-based memory, an ALD deposited Al_2O_3 layer was deposited on the MoO_3 layer to form the bi-layer structure device. The electrical properties of the TiN/Al_2O_3/MoO_3/TiN device are shown in Fig. 4. Unlike the single layer device, a large forming voltage (-12.4 V) was required to initialize the device (shown in the inset image of Fig. 4a). After forming, the device can be switched in both SET process and RESET process by applying DC sweep between ±2 V. Fig. 4a presents the I-V characteristics of the TiN/Al_2O_3/MoO_3/TiN device. Especially, while similar bipolar switching behavior was observed, the bi-layer memristor demonstrates a positive SET behavior where an abrupt change of current was observed when the positive bias reached around +0.8 V and the device was switched to the LRS. Subsequently, when a negative voltage was applied on the top electrode, the device was switched back to HRS at approximately -1.15 V. Fig. 4b demonstrates the endurance of the TiN/Al_2O_3/MoO_3/TiN device with 100 cycles. The resistance was read at 0.1V and it can be investigated that the ratio between HRS and LRS had slightly increased, which reached at around an order of magnitude. In addition, the drift of the HRS and LRS has been significantly reduced. The highly stable retention performance can also be confirmed at room temperature for over 10^3 s, as demonstrated in Fig. 4c. Fig. 4d presents the device to device stability by comparing the HRS and LRS from five randomly selected devices. It shows the resistance states in these devices are controlled in the relatively stable range.

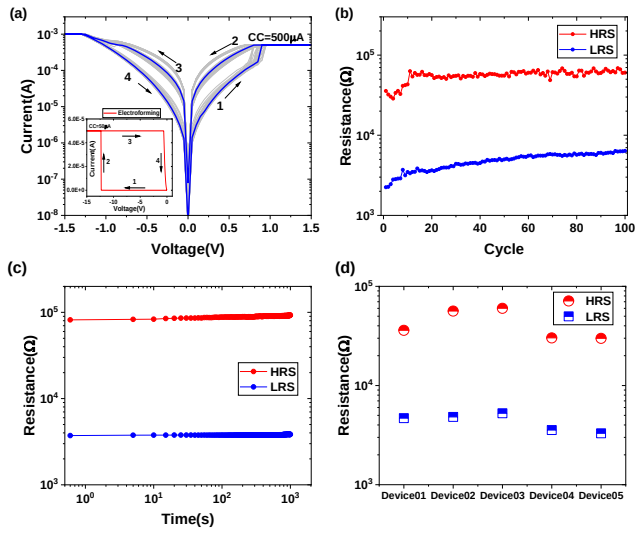

Figure 4. Resistive switching behaviors of the TiN/Al_2O_3/MoO_3/TiN bilayer memory cell. (a) I–V characteristics of the device (inset: electroforming process with a CC of 50 µA); The endurance (b) and retention (c) of the device; (d) Device to device comparison of averaged resistance values in HRS and LRS.

With the purpose of qualitatively understanding the improvement between single layer device and bilayer device, the resistance distribution and voltage distribution of two types of devices are plotted. Fig. 5 illustrates the resistive switching behaviors of TiN/MoO_3/TiN single layer memory cell (marked as SL in the diagram) and TiN/Al_2O_3/MoO_3/TiN bilayer memory cell (marked as BL in the diagram), respectively. Specially, it can be investigated from the Fig. 5a that the ratio between HRS and LRS has improved as the bilayer structure constructed. The resistance of LRS was still distributed in the similar order, while the resistance of HRS increased. Meanwhile, it can be noted that the stability of resistance states are enhanced, as well. In order to precisely and quantitatively describe the how much stability of the device improved, the coefficients of the variation (σ/μ, σ is the standard deviation and μ is the mean value) was introduced in the analysis. The calculated variation coefficients of resistance value in HRS and LRS are 25.7 % and 41.4 % at the single layer memory cell, respectively. Compared with the MoO_3 single layer device, the bilayer device was more stable as the variation coefficients of the resistance value in HRS and LRS are 14.5 % and 21.8 %. Moreover, the Fig. 5b illustrates that the programming voltages of two kinds of devices are controlled in a relatively low voltage range (around ±1.0 V), which is benefit for low-power application. Since the resistive states are more stable, the programming voltages are more uniform when both Al_2O_3 layer and MoO_3 are designed as the dielectric layer. For single layer memory device, it can be observed that the coefficients of the variation of programming voltages are 17.3 % in SET process and 14.9 % in RESET process, respectively. Regarding bilayer memory, those values are calculated respectively as 4.9 % and 3.2 %. Thus, it is an effective method to enhance single MoO_3 based resistive memory electric properties by introducing another dielectric material, such as Al_2O_3.

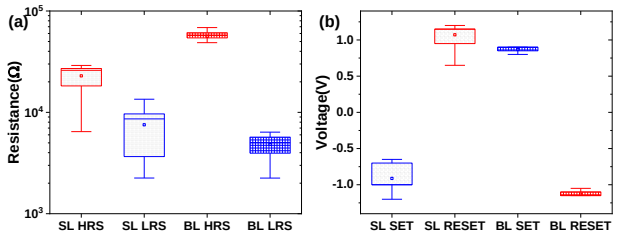

Figure 5. Schematic diagrams of resistive switching behaviors of the TiN/MoO_3/TiN single layer memory cell(SL) and TiN/Al_2O_3/MoO_3/TiN bilayer memory cell(BL) : (a) Resistive distribution; (b) Programming voltage(SET voltage and RESET voltage)distribution.

In order to investigate the possible conduction mechanism of MoO_3 based resistive memories, the SET processes of each device were displayed by replotting the image in the log-log scale in Fig. 6. The logarithmic I–V curve and linear fitting of single layer MoO_3 device are plotted in the Fig. 6a. It is demonstrated that the conduction mechanism in the MoO_3 single layer memory cell can be fitted by the space-charge-limited current (SCLC) model. Specifically, from 0 V to 0.3 V at the HRS, the cell is managed by the standard linear dependence of current with input voltage and the slope of the linear part is around 1.15. It is possible that the mobile electrons are generated by the thermal excitation in this region and display typical Ohmic conduction mechanism. From 0.35 V to 0.6 V, the slope of the linear fitting changes to around 1.87. The Child's square law region is illustrated because the current is generally proportional to the square of applied voltage ($I \propto V^2$). According to the SCLC theory, the $I \propto V^2$ region is defined as the trap-unfilled SCLC region, where the current density can be given by the equation.

$$J_{SCLC} = \frac{9}{8}\varepsilon_i \mu \theta \frac{V^2}{d^3} \quad (1)$$

J is the current density, ε_i is the permittivity of the oxide, μ is the mobility, θ is the ratio of free and shallow trapped charge, and d is thickness of the oxide. After the trap-unfilled region, the conductive filament forms and charges traps in the trap-filled SCLC region, where the slope of the third region is around 4.2. At the threshold of 0.9 V, there is a short abrupt increase drifting the device from HRS to LRS.

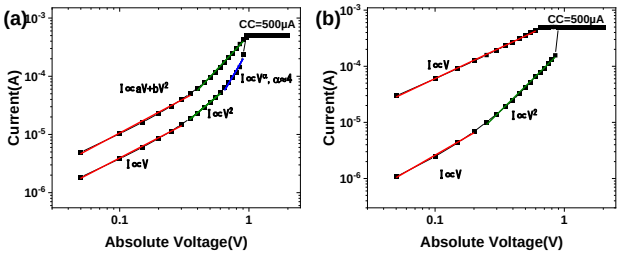

Figure 6. I–V characteristics and the SET process I–V curves in double-logarithmic plots of the (a) single layer TiN/MoO_3/TiN device switched with CC of 500 μA and (b) bilayer TiN/Al_2O_3/MoO_3/TiN device switched with a CC of 500 μA

A similar conduction mechanism is illustrated in the Fig. 6b. As depicted in the linear fitting of TiN/Al_2O_3/MoO_3/TiN bilayer memory cell, the region from 0 V to 0.2 V is governed by the Ohmic conduction mechanism and the higher voltage area presents is SCLC conduction mechanism. At around 0.85 V, there is a significant abrupt current increase, indicating the device comes into HRS from LRS.

According to above discussed conduction mechanism analysis and measured resistive switching properties, the possible schematic of conduction models are proposed in the Fig. 7. For single layer TiN/MoO_3/TiN device (shown in the Fig. 7a-i, there are a few of oxygen vacancies (labelled as V_o in the diagram) existing in the MoO_3 dielectric layer after deposition. When the voltage was applied on the top electrode, the oxygen ions and vacancies could be drifted based on the electric field direction. In this case, the oxygen ions were ionised and drifted towards the bottom electrode due to the electrical field where the TiN could serve as an oxygen reservoir. This generated more oxygen vacancies in the film which drifted towards the top electrode. These oxygen vacancies formed a conductive path between two electrodes, leading to the transition from HRS to LRS(shown in the Fig. 7a-ii). When a reversed polarity of electric field was applied, the oxygen vacancies near the bottom electrode were recombined with the oxygen ions and ruptured the filament. This resulted in the RESET of the device from HRS to LRS (shown in the Fig. 7a-iii).

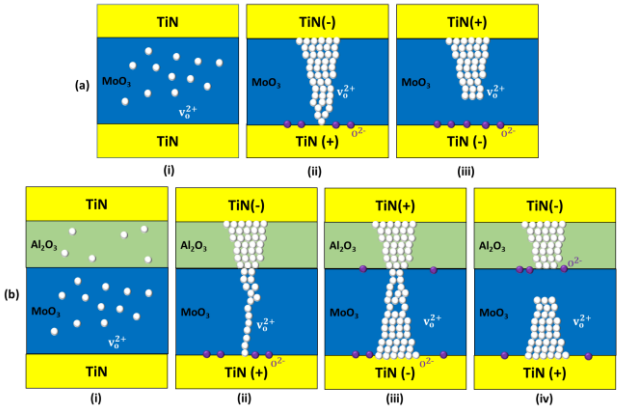

Figure 7. Schematic diagram illustrating bipolar resistive switching mechanism for the single layer TiN/MoO_3/TiN device and the bi-layer TiN/Al_2O_3/MoO_3/TiN device. Black dots represent oxygen vacancies existing in the MoO_3 layer and purple dots represent the oxygen ions.

Regarding the TiN/Al_2O_3/MoO_3/TiN bilayer memory, the switching model is illustrated in the Fig. 7b. The large forming voltage required is likely due to the initialization of the Al_2O_3 layer with less oxygen vacancy, which is shown in the Fig. 7b-i. When the external voltage was applied on the top electrode, due to the high number of oxygen vacancies present in the MoO_3 layer, a confined filament started to develop inside the MoO_3 layer, soon after filament was generated in Al_2O_3 layer. This fixed point filament formation will help in stable performance of bi-layer device. It is likely that these two filaments were linked and connected the top electrode and the bottom electrode. In this case, the filament in the Al_2O_3 layer formed a 'virtual electrode'(shown in the Fig. 7b-ii). When applying positive voltage on the top electrode, the new oxygen vacancies generated and got together at the bottom electrode. The whole filament exhibited an asymmetric structure with the weakest point located in the interface between Al_2O_3 layer and MoO_3 layer. It can be defined that the top electrode and bottom electrode was connected, which can be demonstrated in the Fig. 7b-iii. In this case, the device reached at the compliance current and SET process was obtained. When the RESET happened, filament in MoO_3 layer partially ruptured while keeping most of the parts intact in the Al_2O_3 layer. The rupture is likely to take place at the fragile part of the whole filament due to Joule heating at the Al_2O_3/MoO_3 interface.

IV. Conclusion

In conclusion, the MoO_3 based memristor was developed demonstrating forming-free, bipolar resistive switching behavior. The resistive switching performance can be significantly improved by implementing a bi-layer TiN/Al_2O_3/MoO_3/TiN structure. The introduction of a Al_2O_3 layer in the device leads to improved ON/OFF ratio, endurance, device to device variation and programming voltages. Meanwhile, the large voltage forming process is required in the bi-layer structure device. The current conduction of the MoO_3 based memristor can be fitted using the SCLC model. The switching mechanism is explained by the formation and rupture of oxygen vacancy based filament. The low programming voltage and reproducible switching behaviors obtained from the MoO_3 bi-layer device certainly points towards its further application as non-volatile switching memory and neuromorphic computing devices.

References

[1] M. Bharathi *et al.*, "Effect of Ag doping on bipolar switching operation in molybdenum trioxide (MoO_3) nanostructures for non-volatile memory," *Journal of Alloys and Compounds*, vol. 862, 2021, doi: 10.1016/j.jallcom.2020.158035.

[2] S. R. Patil *et al.*, "Forming-free and multilevel resistive switching properties of hydrothermally synthesized hexagonal molybdenum oxide microrods," *Journal of Materials Science: Materials in Electronics*, vol. 32, no. 9, pp. 12490-12502, 2021, doi: 10.1007/s10854-021-05883-w.

[3] M. C. Sahu, S. K. Mallik, S. Sahoo, S. K. Gupta, R. Ahuja, and S. Sahoo, "Effect of Charge Injection on the Conducting Filament of Valence Change Anatase TiO_2 Resistive Random Access Memory Device," (in English), *J Phys Chem Lett*, vol. 12, no. 7, pp. 1876-1884, Feb 25 2021, doi: 10.1021/acs.jpclett.1c00121.

[4] W. J. Chen, C. H. Cheng, P. E. Lin, Y. T. Tseng, T. C. Chang, and J. S. Chen, "Analog Resistive Switching and Synaptic Functions in WO_x/TaO_x Bilayer through Redox-Induced Trap-Controlled Conduction," (in English), *Acs Appl Electron Ma*, vol. 1, no. 11, pp. 2422-2430, Nov 2019, doi: 10.1021/acsaelm.9b00572.

[5] C. Ye *et al.*, "Enhanced resistive switching performance for bilayer HfO_2/TiO_2 resistive random access memory," (in English), *Semicond Sci Tech*, vol. 31, no. 10, Oct 2016, doi: Artn 105005; 10.1088/0268-1242/31/10/105005.

[6] M. Ismail *et al.*, "Effects of Gibbs free energy difference and oxygen vacancies distribution in a bilayer ZnO/ZrO_2 structure for applications to bipolar resistive switching," (in English), *Applied Surface Science*, vol. 498, Dec 31 2019, doi: ARTN 143833; 10.1016/j.apsusc.2019.143833.

[7] S. K. Vishwanath, H. Woo, and S. Jeon, "Enhancement of resistive switching properties in Al_2O_3 bilayer-based atomic switches: multilevel resistive switching," (in English), *Nanotechnology*, vol. 29, no. 23, Jun 8 2018, doi: ARTN 235202; 10.1088/1361-6528/aab6a3.

[8] J. Wang *et al.*, "A unipolar nonvolatile resistive switching behavior in a layered transition metal oxide," *Nanoscale*, vol. 11, no. 43, pp. 20497-20506, Nov 21 2019, doi: 10.1039/c9nr07456b.

[9] S. L. Fang *et al.*, "Multilevel resistive random access memory achieved by MoO_3/Hf/MoO_3 stack and its application in tunable high-pass filter," *Nanotechnology*, vol. 32, no. 38, Jun 29 2021, doi: 10.1088/1361-6528/ac0ac4.

[10] C. S. Yang, D. S. Shang, Y. S. Chai, L. Q. Yan, B. G. Shen, and Y. Sun, "Moisture effects on the electrochemical reaction and resistance switching at Ag/molybdenum oxide interfaces," (in English), *Physical Chemistry Chemical Physics*, vol. 18, no. 18, pp. 12466-12475, May 14 2016, doi: 10.1039/c6cp00823b.

[11] T. J. Dai, L. X. Qian, Y. X. Ren, and X. Z. Liu, "MoO_{3-x}-based Bipolar Switching ReRAM Fabricated by Atomic Layer Deposition," (in English), *Ieee C Elec Devices*, 2017. [Online]. Available: <Go to ISI>://WOS:000426985900039.

[12] A. Bertuch, G. Sundaram, M. Saly, D. Moser, and R. Kanjolia, "Atomic layer deposition of molybdenum oxide using bis(tert-butylimido)bis(dimethylamido) molybdenum," *Journal of Vacuum Science & Technology A: Vacuum, Surfaces, and Films*, vol. 32, no. 1, 2014, doi: 10.1116/1.4843595.

[13] S. Puebla, A. Mariscal-Jimenez, R. S. Galan, C. Munuera, and A. Castellanos-Gomez, "Optical-Based Thickness Measurement of MoO_3 Nanosheets," *Nanomaterials (Basel)*, vol. 10, no. 7, Jun 29 2020, doi: 10.3390/nano10071272.

[14] J. Fatheema *et al.*, "A comprehensive investigation of MoO_3 based resistive random access memory," *RSC Advances*, vol. 10, no. 33, pp. 19337-19345, 2020, doi: 10.1039/d0ra03415k.

[15] S. Bai *et al.*, "Facile synthesis of α-MoO_3 nanorods with high sensitivity to CO and intrinsic sensing performance," *Materials Research Bulletin*, vol. 64, pp. 252-256, 2015, doi: 10.1016/j.materresbull.2014.12.049.